Finite micro-tab system for load control on a wind turbine

A B Bach[1], M Lennie[1], G Pechlivanoglou[2], C N Nayeri[1] and C O Paschereit[1]

[1] Institute of Fluid Mechanics and Technical Acoustics, Technical University of Berlin, Müller-Breslau Str. 8, 10623 Berlin, Germany
[2] SMART BLADE GmbH, Waldemarstr. 39, 10999 Berlin, Germany

E-mail: alena.bach@tu-berlin.de

Abstract. Finite micro-tabs have been investigated experimentally to evaluate the potential for load control on wind turbines. Two dimensional full span, as well as multiple finite tabs of various aspect ratios have been studied on an AH93W174 airfoil at different chord wise positions. A force balance was used to measure the aerodynamic loads. Furthermore, the wake vortex system consisting of the Kármán vortex street as well as the tab tip vortices was analyzed with a 12-hole probe and hot wire anemometry. Finally, conventional oil paint as well as a quantitative digital flow analysis technique called SMARTviz were used to visualize the flow around the finite tab configurations.
Results have shown that the devices are an effective solution to alleviate the airfoils overall load. The influence of the tab height, tab position as well as the finite tab aspect ratio on the lift and lift to drag ratio have been evaluated. It could be shown, that the lift difference can either be varied by changing the tab height as well as by altering the aspect ratio of the finite tabs. The drag of a two-dimensional flap is directly associated with the vortex street, while in the case of the finite tab, the solidity ratio of the tabs has the strongest effect on the drag. Therefore, the application of a finite tab system showed to improve the lift to drag ratio.

1. Introduction

The rising demand in renewable energy leads to a growth of the worldwide installed wind turbines. Today the globally installed wind power capacity covers 283GW. To accomplish these values, the energy gain per turbine was improved mostly by up-scaling the turbines and enlarging of the rotor diameters. Current large wind turbines yield up to 8MW with a rotor diameter of 160m. The up-scaling of the components however is reaching the technical limits: The blade mass itself is already substantially straining the blade structure, the pitching mechanism is relatively slow for such a massive blade and the bearing structure has to deal with huge loads. Furthermore, the aerodynamic loads caused by the unsteady inflow add to the problem: A larger rotor diameter encounters stronger fluctuating loads due to the earth boundary layer and yaw misalignment. The tower shadow and the local gusts induce further disturbances. These effects are the cause for fatigue loads, which reduce the overall lifetime of wind turbines and consequentially increase the costs of energy.
Active load control is considered as one solution to deal with fatigue loads and has been studied in the past as an additional application on wind turbines [1]. Possible control techniques which

Content from this work may be used under the terms of the Creative Commons Attribution 3.0 licence. Any further distribution of this work must maintain attribution to the author(s) and the title of the work, journal citation and DOI.
Published under licence by IOP Publishing Ltd

are mostly known from the aviation and helicopter industry are e.g. suction and blowing mechanisms, zero-mass actuators or movable parts such as trailing or leading edge flaps. Various approaches have been considered for the application on wind turbines in the last years. In this context the micro-tab system was regarded as an appropriate and promising solution [2].

2. Theoretical Background of Micro-Tabs

Micro-tabs are small devices, which are generally placed between 90% chord length and the trailing edge and deploy perpendicular to the airfoils surface (see Figure 1). Thereby, the size of the tabs usually is in the order of the local boundary layer thickness. The presence of the tab changes the flow pattern at the trailing edge by effectively changing the chamber distribution and hence the lift [2]. Depending on their placement either on the upper or lower side of the airfoil load reduction or load enhancement can be obtained over a wide range of angles of attack. A further advantage is that the non-deployed micro-tabs retract completely inside the blade without any disturbance of the flow. Next to this, the tabs can be integrated in the blade without requiring substantial changes in the blade manufacturing process [3]. In summary, the short tabs are generally cost effective, provide significant control authority and require low energy input when used as an active load control system and have been used for numerous applications [4] [5] [6] [7]. All the above mentioned reasons make them particularly interesting for the application on wind turbine blades to reduce fatigue loads.

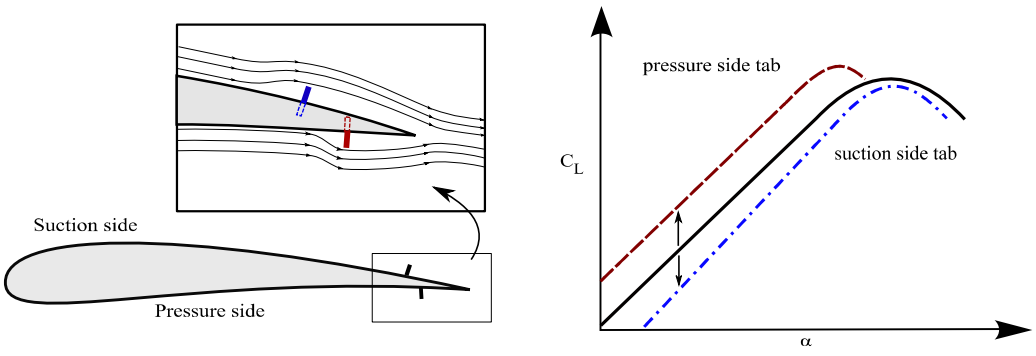

Figure 1: Micro-tab concept

3. Experimental Setup

Experimental investigation in the wind tunnel has been conducted on an Althaus AH93W174 wind turbine profile with passive micro-tabs. The measurement section of the wind tunnel has a size of 1.5m x 2m with a turbulence level of $Tu < 0.5\%$. For a better two-dimensionality, additional splitter plates were installed between the model and the wind tunnel wall. The chord length of the profile was $c = 0.6m$, the span was $y = 1.44m$. Measurements were performed at a Reynolds number between $Re = 8 \cdot 10^5$ and $Re = 1 \cdot 10^6$. Wind tunnel correction methods for solid blockage, wake blockage and the effect of streamline curvatures were used. The flow was tripped on the upper surface at $x/c = 15\%$. This was done to see the impact of the tabs with an increased boundary layer height. This is because environmental effects cause a much larger roughness on exposed wind turbines and hence the boundary layer height is generally much larger than for the clean airfoil.
For the study various tab configuration were installed and tested. Thereby, the tabs were placed close to the trailing edge between $90\% \leq x/c \leq 100\%$ and varied in height from

$1\% \leq h_{tab}/c \leq 4\%$. Furthermore, the difference of a full span tab and multiple smaller tabs were investigated. The solidity ratio was introduced in the following way: $\sigma = \Sigma(l_{tab})/y$. A full span tab has the solidity ratio of $\sigma = 1$. For the experimental investigation of the micro-tab concept different measurement approaches have been chosen. First of all, a 6-component force balance underneath the wind tunnel measured the aerodynamic forces. Second, a hotwire was used to evaluate underlying frequencies in the wake. The single-wire had a measurement sampling rate of $f = 2000Hz$ and was placed $\Delta x = 20mm$ behind the trailing edge. Third, measurements with a 12-hole probe have been carried out in the same plane in the wake in order to analyze the extent and interaction of the tab's streamwise vortices. Finally, oil paint as well as a quantitative digital flow analysis technique based on flow tufts (SMARTviz) visualized the flow around various finite tab configurations.

4. Static Full Span Micro-Tab

The following section shows the experimental results for passive micro-tabs placed along the full span. The tabs's height as well as chordwise positions were varied in order to better understand the effects on lift and drag.

4.1. Influence of Tab Height

Lift and drag curves have been measured for the tab placed on the pressure side and on the suction side directly at the trailing edge with $x/c = 100\%$ and the polars were compared to the tripped baseline case. Thereby, the tab height was varied between $1\% \leq h_{tab}/c \leq 4\%$.
Figure 2 shows the lift curves for tabs placed on the pressure side as well as the baseline. The flat lift gradient is due to the boundary layer trip. The main observation is that the tab shifts the curve to higher lift values and changes the angle of attack where stall occurs to smaller inflow angels. This is due to the fact that the tab acts as if the camber of the airfoil is raised and hence the airfoils stalls at lower angles of attack. Furthermore, the tab with a not sufficient tab height of $h_{tab} = 1\%c$ does not follow this pattern but stalls at very low angles and actually produces less lift in the post stall region.

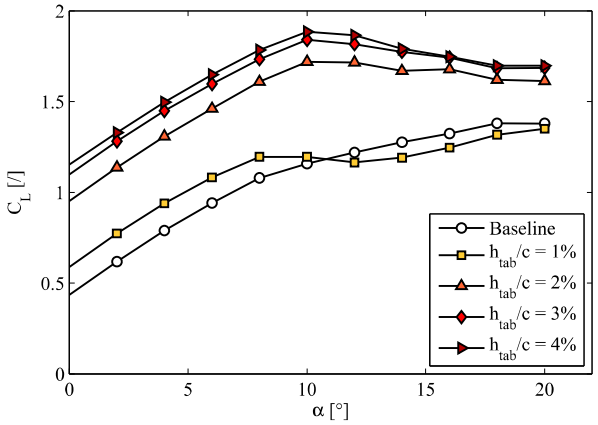

Figure 2: Lift curve for various micro-tabs at the pressure side at $x/c = 100\%$ ($Re = 8 \cdot 10^5$).

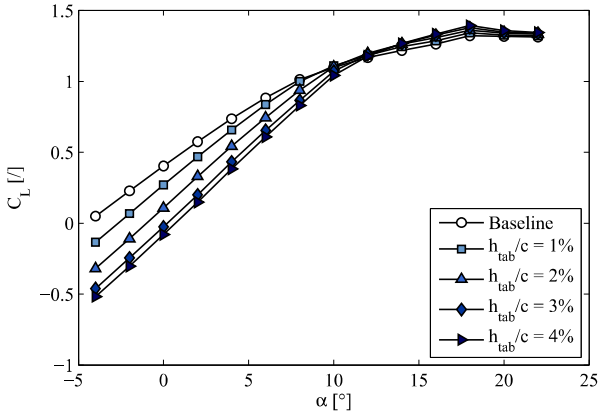

Figure 3: Lift curve for various micro-tabs at the suction side at $x/c = 100\%$ ($Re = 8 \cdot 10^5$).

For the tab on the suction side, the lift decrease is less pronounced if the angle of attack is increased (see Figure 3). If the profile stalls, the lift decrease is canceled out and its effect is even reversed to a slight lift increase. The latter can also be observed in the measurements

by e.g. Nakafuji [8]. This behavior has not yet been completely understood, since it was not consistently observed by involved researchers. However, flow visualization suggest that the tab placed on the suction side does reduce the effect of the necklace vortices as well as postpone the onset of stall to higher angles of attack. This effect is of course critical for the load control reduction mechanism and is a subject of ongoing research.
The tab influence on the airfoil's drag is visible in Figure 4 and 5. Obviously, a larger tab results in overall higher drag. Whereas for the tab on the pressure side the drag is slowly rising for prestall angles, the drag of the suction side tab is slightly reduced with rising angle of attack before stall.
Which tab configuration is most advantageous depends not only on the lift but also on the drag characteristics. Regarding the best lift to drag ratio (L/D) of all configurations and comparing these with the baseline case yield the values listed in Table 1. One can see, the reduction in the L/D ratio is still small especially for the 1% and 2% tab heights. Furthermore, the reduction of the L/D ratio seems to be generally less pronounced for the tab placed on the pressure side.

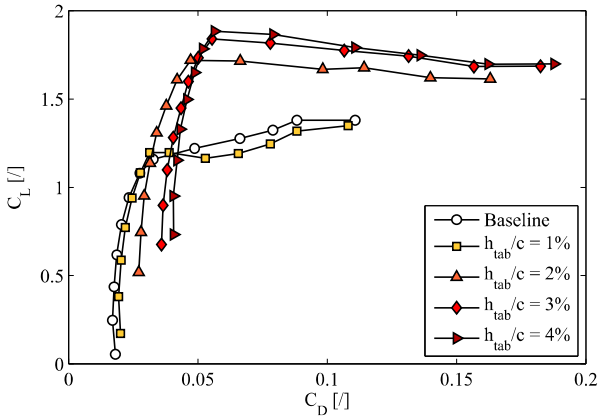

Figure 4: Drag curve for various micro-tabs at the pressure side at $x/c = 100\%$.

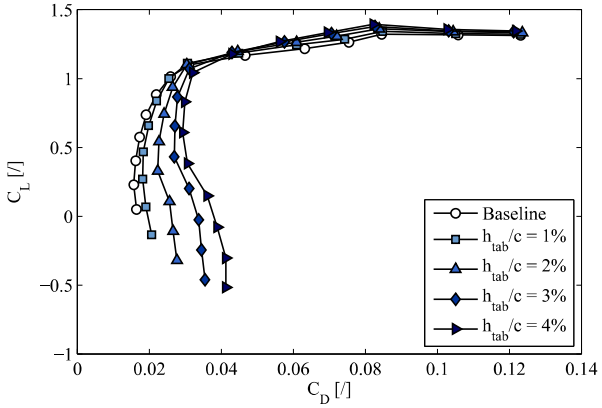

Figure 5: Drag curve for various micro-tabs at the suction side at $x/c = 100\%$.

h_{tab}/c [%]	$(L/D)_{PS,max}/(L/D)_{base,max}$ [/]	$(L/D)_{SS,max}/(L/D)_{base,max}$ [/]
1	0.948	0.957
2	0.941	0.880
3	0.839	0.836
4	0.835	0.789

Table 1: L/D ratio as a fraction of the baseline L/D ratio for the airfoil with various tab height on pressure (PS) and suction side (SS).

4.2. Influence of Tab Position
It was shown, that not only the tab height but also the chordwise tab position on the airfoil has an effect on the lift. The best tab position depends on the inner space of each profile as well as the aerodynamic gain which can be achieved. Figure 6 and 7 show the lift increase for all four tab heights placed between 90% and 100% of the chord length close to the trailing edge. It can be seen, that for the tab on the pressure side, a placement further upstream of the trailing edge is disadvantageous for the lift gain. The slope of the lift gain for the 2%, 3% and 4% high tab

is comparable. The 1% high tab, which already showed a different behavior in the lift curve in Figure 2, reaches a negative value for a placement at 90% chord. This means, that the tab's early stall behavior as observed in Figure 2 is precipitated to even lower angles of attack. For a tab placement on the suction side there seems to be a slight advantage of moving the tab upstream Figure 7. However, for the tripped Althaus profile the effect is nearly negligible.
The best tab position is based on the inner profile space available for the tab's integration as well as the lift and drag characteristics. For the Althaus profile with a sharp trailing edge, this would only allow a tab height of $h_{tab}/c = 1\%$ at $x/c = 95\%$ and $h_{tab}/c = 2\%$ at $x/c = 90\%$. These values improve slightly when the airfoil shape is modified by applying a certain pre-set thickness at the trailing edge.

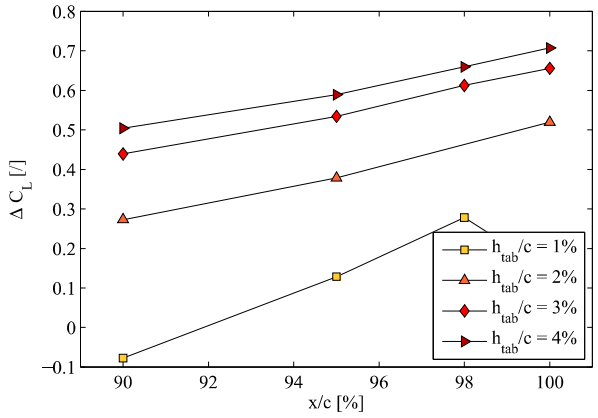

Figure 6: Lift increase at $\alpha = 6$ for various chordwise tab positions for a tab placement on pressure side

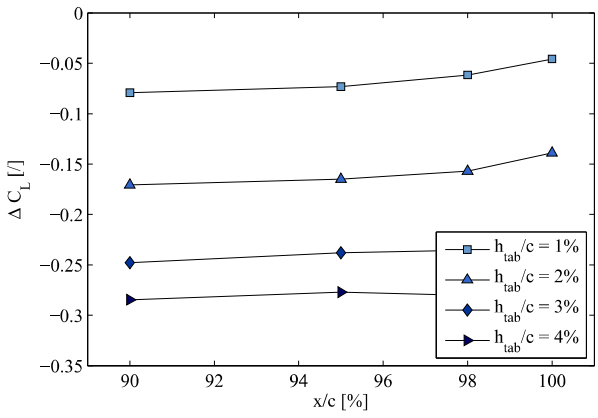

Figure 7: Lift reduction at $\alpha = 6$ for various chordwise tab positions or a tab placement on suction side

4.3. Wake Vortex Street
The formation of a vortex street behind the tab is one major reason for the drag of the tab and furthermore causes a time dependent variation of the lift [9]. Hotwire measurements have been carried out to analyze the dominant frequency of the vortices $\Delta x = 20mm$ behind the tab placed at the trailing edge. Different tab sizes on the suction side and the pressure side were investigated as well as the dependency of the Strouhal number of the current angle of attack. The Strouhal number was based on the tab height and the velocity of the incoming flow: $St = f \cdot h_{tab}/U_\infty$. It was found, that the higher the tab is, the smaller the frequency becomes and hence the larger the Strouhal number is (Figure 8). Furthermore, the Strouhal numbers for the suction side tab were found to be around $\Delta St = 0.05$ higher for the pressure side tab. This can be explained with the difference in the boundary layer at the suction side and at the pressure side. The boundary layer is thicker at the suction side and hence the tab is within a region with smaller velocities which cause a larger Strouhal number.
The boundary layer thickness is not only dependent on the chordwise position and the side of the profile but also on the angle of attack. Hence, the Strouhal number must also change according to the current inflow angle. Figure 8 shows how the Strouhal number is influenced by the angle of attack for a tab height of $h_{tab}/c = 4\%$. Additionally, the displacement thickness of the boundary layer is plotted as calculated by QBlade based on the XFOIL code [10]. Again, the Strouhal number for the tab on the suction side is found to be larger than for the pressure side for all angles of attack. The boundary layer thickness on the suction side is rising with

the angle of attack, which is accompanied by a rising Strouhal number for the suction side tab. However, the amplitude of power density signal of the vortex street became less pronounced for the higher angles of attack. Finally, at the onset of stall at $\alpha = 10$, the signal was weak and the Strouhal number dropped. For an angle of $\alpha = 12°$ no dominant frequency was found in the wake for the suction side tab, whereas the Strouhal number for the pressure side tab was found to have an opposite effect. The boundary layer gets thinner, the higher the angle is and hence the Strouhal number gets smaller.
The vortex street is not only responsible for additional drag but as well a possible source of noise on the blade section. A good indicator for the noise is the amplitude of the peak in the power density spectrum. For the tab on the pressure and section side it was observed that the amplitude of the signal increased together with the tab height. This indicates a higher noise for the higher tab. Furthermore, the amplitude decreased with rising angle of attack. On a real turbine with static, non-moving tabs, placed at the outer section, one can estimate a wake frequency of $f_{SS} \approx 160Hz$ for the tab on the suction side and $f_{PS} \approx 120Hz$ for the pressure side (assuming $U_{rel} = 80m/s$, $c = 2.5m$ and $h_{tab}/c = 4\%$). However, since the tabs are not going to be fixed in its position but actively deploying during each rotor revolution, an exact answer is hard to estimate.

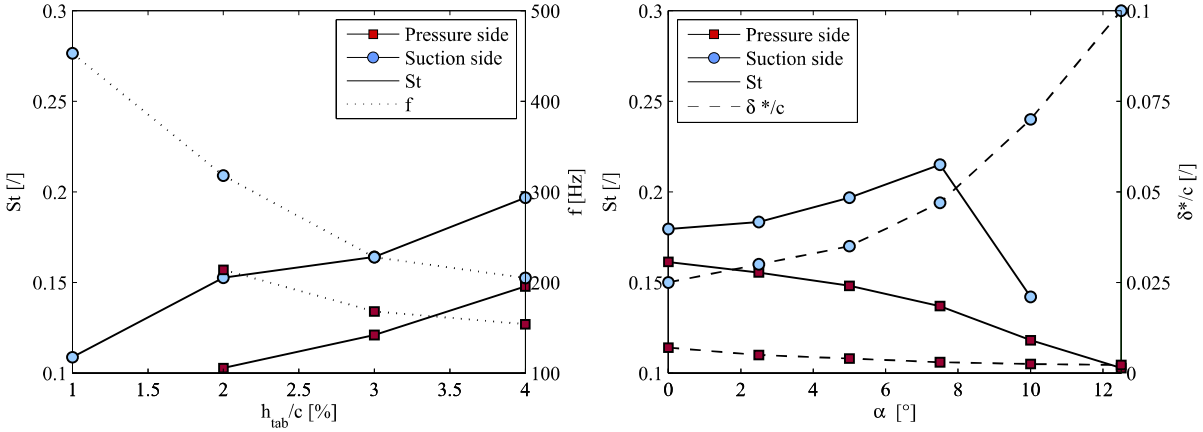

Figure 8: Strouhal number dependency of h_{tab} for $\alpha = 5°$ (left) and the angle of attack for $h_{tab}/c = 4\%$ (right)

5. Finite Micro-Tab

In an attempt to reduce the drag and improve the L/D ratio, serrated as well as multiple finite micro-tabs have been studied in the past [3]. In the following section the effects of multiple finite micro-tabs are presented as an alternative aerodynamic control concept. For a tab height of $h_{tab}/c = 2\%$ various measurement have been carried out with different solidity ratios applied. Thereby, the tab length l_{tab} was varied as well as the length of the gap l_{gap} between the tabs.

5.1. Lift and Drag

The solidity ratio was varied between $\sigma = 0.5$ which corresponds to the baseline case and $\sigma = 1$ which corresponds to the full span configuration. In Figure 9 the lift difference normalized with the difference gained with the full span configuration (FS) is presented. It shows, that for the same solidity ratio but different tab sizes similar results were found for tabs placed on the same profile side. The tabs lift gain depend more or less linearly on the solidity ratio. Thereby, the suction side tabs suggest that a section with $\sigma = 0.8$ corresponds to approx. 80% lift of the full

span configuration. However, this behavior is not found for the tabs on the pressure side, where the lift decays linear, but the loss in lift is more pronounced due to the usage of finite tabs. The corresponding L/D ratio in respect to the L/D ratio of the full span configuration is presented in Figure 10. One can see, that the finite pressure side tabs result in a much better L/D ratio than the full span configuration. However, this result cannot be achieved for the finite tabs on the suction side. Here the L/D ratio was within the same range as the full span configuration. For both airfoils sides it can be observed that the solidity ratio between $\sigma = 0.66 - 0.9\%$ had a negligible effect on the lift to drag ratio.

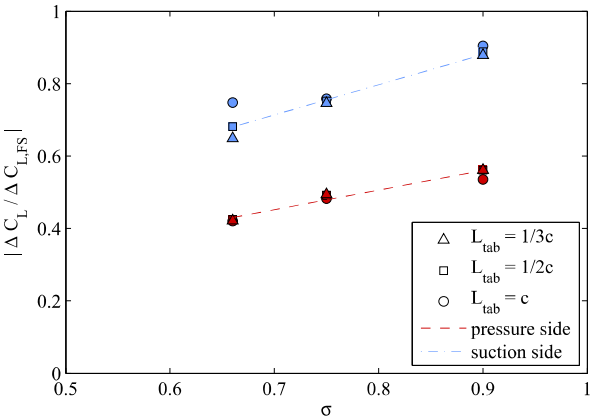

Figure 9: Normalized lift difference dependent on the solidity ratio (x/c=98%)

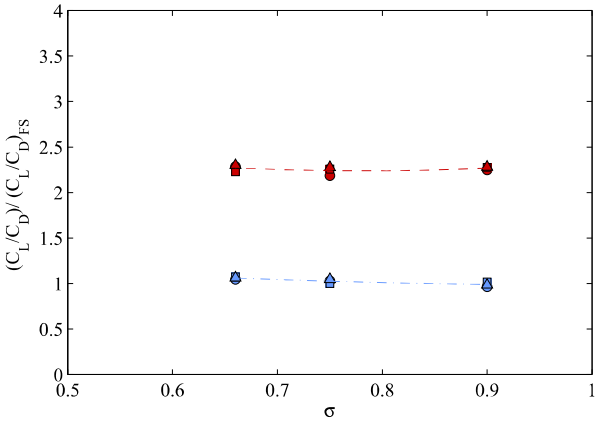

Figure 10: Normalized lift/drag ratio dependent on the solidity ratio (x/c=98%)

Therefore, if these curves are known for a profile with a fixed set of tabs which can be deployed individually, a method is found to alleviate the airfoil's lift without changing the tabs height. This is an advantage to control aerodynamic loads. The positioning of the correct tab height is more difficult to accomplish since highly accurate motor control systems are needed. Whereas a system built out of multiple tabs based on a simple on/off system would be more stable, cost efficient and accurate in its positioning and would therefore requires less maintenance [11]. The multiple tabs offer a better lift to drag ratio than a full span version due to the flow passage offered by the gap.

5.2. Flow Field

The flow field around the finite micro-tab is characterized by the flow through the gaps between the finite tabs. This bypass stream reduces the overall drag. The flow field around the tab has been analyzed with oil paint as well as a quantitative tuft flow visualization technique that was developed at TU Berlin in cooperation with SmartBlade GmbH [12]. The wing is equipped with flow indicators and image registration markers. Using a high-resolution digital camera the individual tufts orientations are tracked using 500 images. Using this data the mean tuft-orientations and their respective standard deviations were calculated. In order to visualize the surface flow patterns, the data was interpolated and a line integral convolution (LIC) was performed. Additionally, the contours of the tufts standard deviations were plotted. The red shading indicates regions of large flow angle variations. The LIC pattern has a visual appearance that is comparable to the oil flow visualization technique.

Figure 11 shows the flow around micro-tabs placed on the suction side at $x_{tab}/c = 90\%$ with a height of $h_{tab}/c = 2\%$ for an angle of attack of $\alpha = 5°$. The two pictures at the left hand side are the results of the oil paint flow visualization which are compared to the results from the flow

tufts found on the right hand side. Both measurements were performed without boundary layer tripping present. In the first row the flow field around a tab with the length of $l_{tab} = 400mm$ is depicted. The second row shows both, measurement techniques used for multiple tabs with the tab length of each $l_{tab} = 200mm$, and an overall solidity ratio of $\sigma = 0.5$. The oil paint visualization on the left hand side shows a laminar separation bubble at around 45% of the chordlength. The absence of the laminar separation bubble in the tuft flow visualization can be explained by the early boundary layer tripping caused by the intrusive flow tufts. However, both measurement techniques show the flow evasion around the tab as well as the separation right before and behind the tab where the recirculation zones are present. For the visualization with the multiple tabs, it is noted that more fluid passes through the gaps between the tabs than surpassing over the tabs. As a consequence, one can see a strong upstream effect of the tabs on the standard variation of the flow direction.

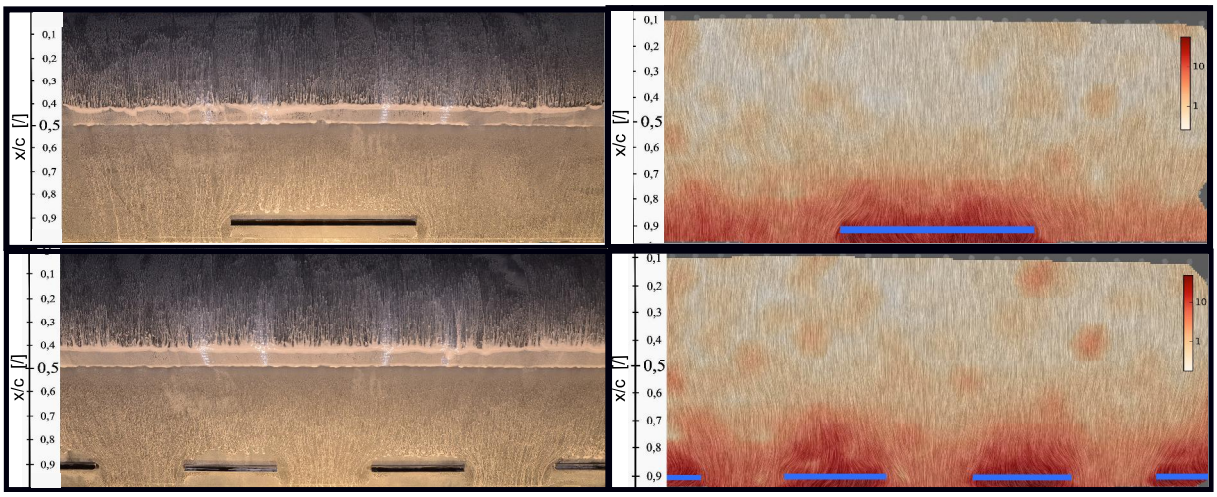

Figure 11: Flow visualization from oil paint (left) and LIC calculation (right) from flow tuft measurement with the standard variation of the local flow direction ($Re = 1 \cdot 10^6$)

Additionally, streamwise vortices form at the tab tips. 12-hole probe measurements were conducted for the same angle of attack of $\alpha = 5°$ in the wake $\Delta x = 20mm$ behind the trailing edge to evaluate the tip vortices. Figure 12a shows the vortices for the tab placed at the trailing edge on the pressure and suction side. Whereas the vorticity is positive for the tab on the pressure side, the vorticity for the suction side tab is negative and less pronounced. In a second study, the vortex interaction of two adjacent tab tip vortices was investigated. Therefore, two tabs with the same height and length were placed at the trailing edge on the pressure side with varying gap sizes with an solidity ratio of $\sigma = 0.75$ and $\sigma = 0.9$ (Figure 12b). The vortex pairs for both configurations are less pronounced and displaced by the presence of the counter-rotating vortex in comparison to the tip vortex of the single tab. Hence the larger the solidity ratio, the smaller the vortex pair becomes in its size and strength.

6. Micro-Tab System for Wind Turbines

In the following section the measurement results are used to simulate the effect of micro-tabs on a wind turbine. The possible change in the flapwise blade root moment with applied micro-tabs will be presented as well as the forces and stresses along the blade. The aim is to reduce the fatigue loading and enhance the overall turbine lifetime. It has to be noted that the trailing

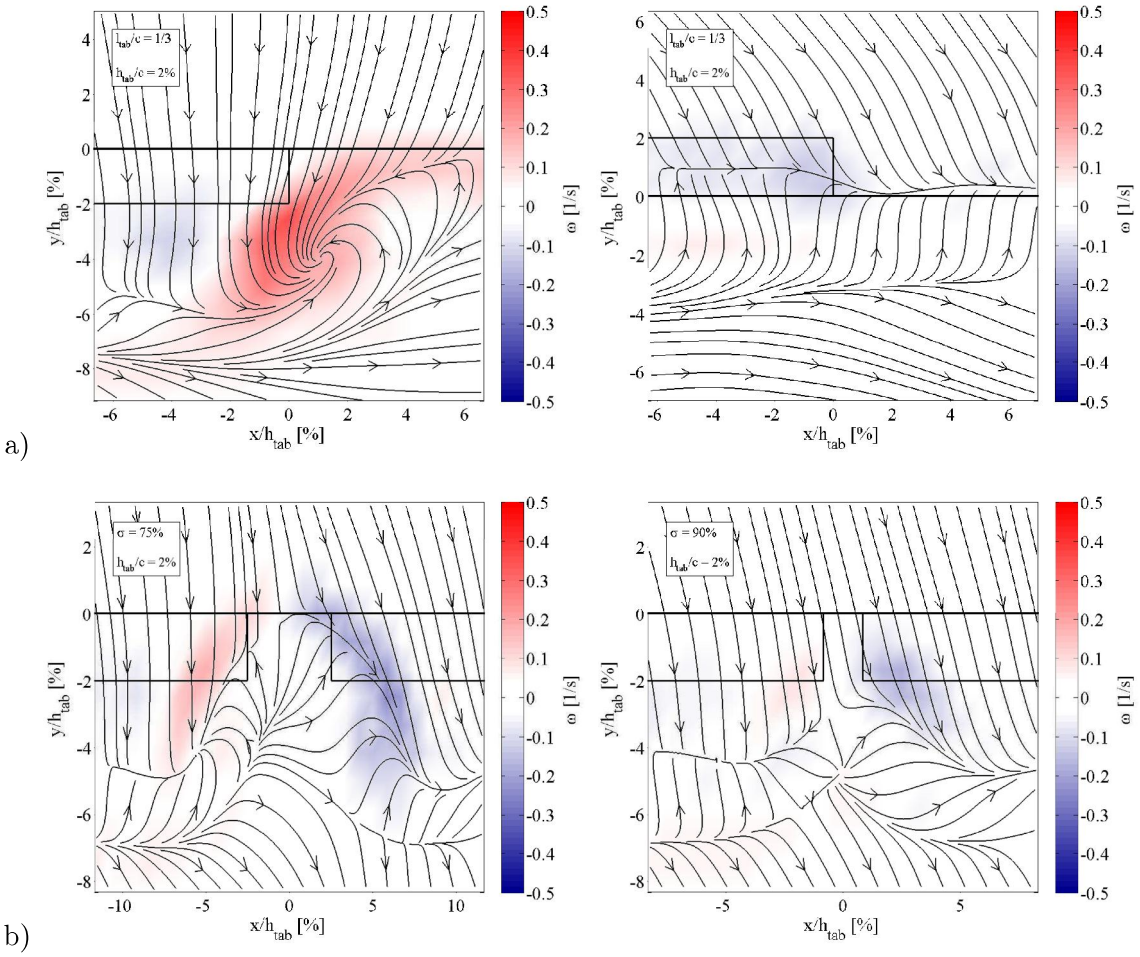

Figure 12: Vorticity field for different finite tab configurations

edge devices represent an additional control for the faster time dependent blade loads but cannot work as a pitch replacement [11].

6.1. Impact of Micro-Tabs on the Blade Loads

To evaluate the best spanwise position and length of the micro-tab system on the blade, multiple simulations were conducted based on the setup of the NREL 5MW research turbine [13]. The turbine was simulated with QBlade, a blade element momentum code (BEM) with various integrated correction algorithms. The NREL turbine setup was modified in a way that the NACA profiles at the outer sections were replaced with the Althaus profile and the experimentally gained results of the force measurements. The chord and twist distribution remained the same. Of course this results in an aerodynamically not optimal designed rotor; however it is sufficient enough to get an impression of the load alteration due to the tab deployment. For the simulation both cases with tabs on the suction as well as the pressure side are considered. For an overall load reduction on the blade section, the local tabs should provide the lift reduction as well as enhancement to stabilize the blade.

For a direct comparison of the effect on the load reduction and enhancement on the blade, the configuration with a tab height of $h_{tab}/c = 2\%$ placed and a chordwise position of $x/c = 100\%$

was chosen for the tabs of the suction side as well as the pressure side. To investigate the maximum effect of the tabs on the flapwise bending moment a solidity ratio of $\sigma = 1$ was used. The tab section started at the blade tip and the overall tab section length was gradually increased in direction of the hub.
In can be seen in Figure 13 that the flapwise blade root bending moment is increasing with a larger tab. However, as the tab reached a length of around 30% of the blade length the bending moment more or less converges. Therefore, with tabs on the outer 30% of the blade and a solidity ratio of $\sigma = 1$ on the suction side one can gain maximal -13% reduction of the bending moment, whereas tabs on the pressure side can yield up to around +25% difference. Hence, this represents the control authority within this setup to reduce the fatigue loads. The blade root flapwise bending moment is generally easy to measure and monitor and can be used as an input control parameter to keep the root bending moment as constant as possible by alleviating the blade loads with an active micro-tab system.

To calculate normal forces and stresses along the blade span a basic FEM study was performed. The sectional properties and isotropic material properties were reverse engineered from the modal frequencies and blade mass. A good agreement for the first flap mode was found with the values stated in the Dowec study on which the NREL 5MW turbine is based [14]. The second flap and first edge modes had a larger variance which was still under 15%. The resulting sectional properties were used as the basis for the static FEM solution.
The FEM solution is linear, static and is restricted to small deformations. The blade was discretized using tapered Euler-Beam elements with secondary terms included to account for rotational effects [15]. The back-stresses were calculated over the sections assuming ideal 3D Euler Beam behavior. These methods assumptions were made in the context of a low fidelity comparison case.

Figure 14 illustrates the calculated normal force coefficient along the blade. The baseline looks smooth in the intersection of the original NREL rotor geometry and the modified Althaus tip sections. The unusual peak of the normal forces at the inner rotor at around 20% of the blade is a characteristic of the original NREL blade geometry. The normal force coefficient at the outer tab section is changed simultaneously throughout the tab's region. This goes along with larger values for the normalized von Mises stresses σ_x at the blade tips which can be seen below. The stresses were normalized with the tensile strength of a reinforced glass fiber material $\sigma_t = 188 \cdot 10^6 Pa$ and hence a value of $\sigma_x = 1$ represents a structural failure. The stresses are found be be the highest at the blades tip, in case the micro-tabs are positioned on the pressure side to enhance the local load. One can further observe that the tab placement on the suction side reduced the stresses in comparison to the baseline case. Since the stresses never exceed a value of around $\sigma_x = 0.15$ the conventional structure can be regarded as sufficient for the integration of micro-tabs.

7. Conclusion

A micro-tab control system for aerodynamic loads along the blade span was presented. The effect on lift and drag depending on the tab height, the chordwise position as well as the solidity ratio for multiple tabs was investigated. Thereby, the higher tab generally produced a greater lift difference as well as higher drag. Furthermore, a more upstream position (x/c) of the suction side tab was found to be advantageous. However, pressure side tabs yielded a better solution if placed closer to the trailing edge. In addition, multiple finite flaps were studied. It was shown, that the loads can be altered by either changing the tab height or by using multiple tabs with adaptable solidity ratio. The control with multiple tabs are easier convertible when it comes to the mechanical parts since it can be based on a simple on/off mechanism.
Furthermore, the impact of spanwise micro-tabs on a wind turbine blade was evaluated. The

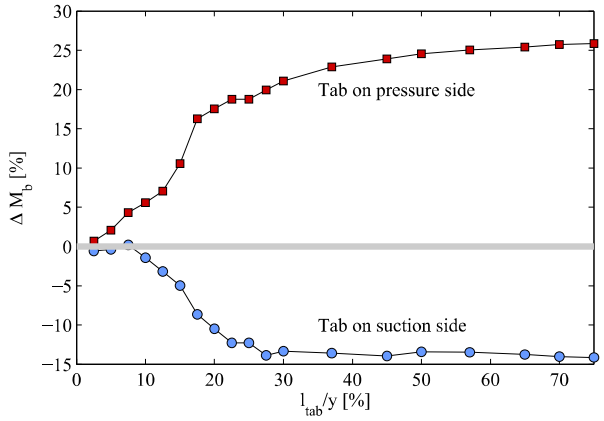

Figure 13: Blade bending moment dependent on the tab section length (measured from the tip)

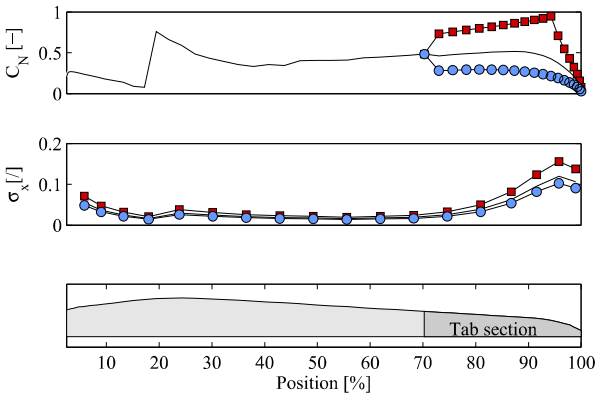

Figure 14: Normal force and von Mises stresses along blade with tabs at the outer 30% of the rotor

blade root bending moment could be altered up to -13% and +25% for the tabs on the suction and the pressure side, respectively. Finally, the normal forces as well as the von Mises stresses along the blade were found sufficiently low for the structural integration of micro-tabs in the blade.

8. Acknowledgments

I would like to acknowledge the support of Stefan Vey for the LIC flow visualization as well as SMARTBLADE for providing the Althaus test wing for the measurements.

References

[1] Barlas T K 2007 State of the Art Prospectives and of Smart Rotor Control for Wind Turbines *J. Phys.: Conf. Series* **75**
[2] Yen D T 2001 Active Load Control for Wind Turbine Blades Using MEM Translational Tabs *ASME Wind Energy Symp.*
[3] Mayda E A 2005 Computational Investigation of Finite Width Microtabs for Aerodynamic Load Control *AIAA Conf.*
[4] Jeffrey D 2000 Aerodynamics of Gurney Flaps on a Single-Element High-Lift Wing *J. of Airc.* **37** 295-301
[5] Myose R 1996 The Effect of Gurney Flaps on Three-Dimensional Wings with and without Taper *SAE Tech. Rep.*
[6] Bieniawski S 2003 Development and Testing of an Experimental Aeroelastic Model with Micro-Trailing Edge Effectors *AIAA Conf.*
[7] Greenblatt D 2009 Flap Vortex Management Using Active Gurney Flaps *AIAA J.* **47** 2845-2856
[8] Nakafuji D T 2002 Load Control for Turbine Blades - A Non Traditional Approach *AIAA Collec. of Tech. Papers*
[9] van Dam C P 2007 Computational Investigations of Small Deploying Tabs and Flaps for Aerodynamic Load Control *J. Phys.: Conf. Series* **75**
[10] Marten D 2010 Integration of a WT Blade Design Tool in XFOIL/XFLR5 *Proc. DEWEK*
[11] Pechlivanoglou G 2012 Passive and Active Control Solutions for Wind Turbines *PhD thesis (TU Berlin)*
[12] Vey S 2014 Quantitative Surface Flow Visualization on Wind Turbines *J. Phys.: Conf. Series* **75**
[13] Jonkman J 2009 Definition of a 5-MW Reference Wind Turbine for Offshore System Development *NREL Tech. Rep.*
[14] Lindenburg C 2002 Aeroelastic Modeling of the LMH64-5 Blade *Tech. Rep.*
[15] Lennie M 2014 Development and Validation of a Modal Analysis Code for Wind Turbine Blades *ASME Conf. Proc.*